land

MDPI

Article

Assessing and Modelling Soil Organic Carbon Dynamics in a Mining Spill Restoration Area from 1998

Javier Bravo-García [1,*], Juan Mariano Camarillo-Naranjo [2], Francisco José Blanco-Velázquez [1] and María Anaya-Romero [1]

[1] Evenor-Tech (Spain), 41011 Seville, Spain; fj.blanco@evenor-tech.com (F.J.B.-V.); m.anaya@evenor-tech.com (M.A.-R.)
[2] Department of Physical Geography and Territorial Analysis, Universidad de Sevilla, 41004 Seville, Spain; jmcamarillo@us.es
* Correspondence: j.bravo@evenor-tech.com

Abstract

Reliable quantification of soil organic carbon (SOC) change is essential for evaluating long-term restoration trajectories and constraining the potential contribution of restored soils to atmospheric CO_2 mitigation. However, long-term SOC monitoring based exclusively on field measurements is often limited by data scarcity, spatial heterogeneity and the high cost of repeated sampling. This study assesses the potential of combining field observations, remote sensing-derived proxies and process-based modelling to simulate SOC dynamics in the Guadiamar Green Corridor, Seville, Spain, a restored area affected by the 1998 Aznalcóllar mining spill. SOC dynamics were simulated using the RothC model under a set of boundary condition scenarios, in which field-measured or locally observed input variables were progressively replaced by alternative data sources. The reference scenario was based mainly on field SOC and clay measurements and local meteorological records, while the remaining scenarios tested the use of NDVI-derived carbon inputs, satellite-derived and reanalysis-based climate variables, and SoilGrids-derived estimates of SOC and clay content. The simulations were evaluated against field observations collected over the restoration period. Overall, RothC reproduced the general direction of the surface-layer SOC decline observed in the monitoring plots, although most scenarios did not fully capture the magnitude of SOC loss measured in the field. Differences among boundary conditions highlighted the sensitivity of RothC to specific input variables, particularly initial SOC, clay content and evapotranspiration. Scenarios based on alternative soil datasets showed that global soil products can provide useful information where field data are limited, but their performance depends strongly on their agreement with local soil conditions. Similarly, the replacement of local climatic data with remote sensing or reanalysis products affected model outputs, especially when evapotranspiration was substituted. These results indicate that satellite-derived products, climate reanalysis and open-access environmental datasets can complement field measurements in SOC modelling, particularly in data-scarce restoration contexts. However, their use requires careful validation, as model accuracy depends on the variable being replaced, the quality of the proxy dataset and the calibration of RothC to plot-specific conditions.

Keywords: boundary conditions; carbon dynamics; remote sensing; RothC; SOC modelling

Check for updates

Academic Editors: Amrakh I. Mamedov and Claude Hammecker

Received: 25 May 2026
Revised: 21 July 2026
Accepted: 24 July 2026
Published: 30 July 2026

Copyright: © 2026 by the authors. Licensee MDPI, Basel, Switzerland. This article is an open access article distributed under the terms and conditions of the Creative Commons Attribution (CC BY) license.

1. Introduction

Soil organic carbon (SOC) is a fundamental component of terrestrial ecosystems, playing a crucial role in soil health, agriculture, the global carbon cycle, and climate change [1]. It has been estimated that SOC accounts for around 25% of the potential of natural climate solutions, although approximately 60% of this potential corresponds to the restoration of depleted stocks [2]. Multiple benefits arise from soil carbon sequestration, including (1) the formation, protection, and remediation of soils and sediments, (2) regulation of risks and extreme events, (3) climate regulation, and (4) the creation and maintenance of habitats; all of which are aligned with the United Nations Sustainable Development Goals (SDGs) [3].

SOC dynamics are controlled by the balance between organic carbon inputs, decomposition, stabilisation and losses through erosion or leaching. Soils do not accumulate carbon indefinitely as their stocks tend to approach a dynamic equilibrium determined by climate, vegetation, soil properties and management [4,5]. This behaviour may be particularly complex in restored or heavily disturbed ecosystems. Mining activities, contaminant removal, soil excavation and the application of mineral or organic amendments can abruptly modify soil structure, texture and carbon stocks [6]. Consequently, the SOC measured shortly after restoration may represent a transient condition rather than a stable baseline, and subsequent decreases do not necessarily indicate renewed ecosystem degradation. They may instead reflect the mineralisation and redistribution of recently incorporated organic matter and the gradual development of a new soil equilibrium [7,8].

Reliable assessment of these long-term changes usually requires repeated field sampling. However, conventional SOC monitoring is constrained by the cost of laboratory analyses, strong spatial heterogeneity, differences in sampling depth and bulk density, and the difficulty of maintaining comparable sampling designs over several decades [3,9]. These constraints are particularly relevant in restored landscapes, where amendments and soil reconstruction can generate pronounced small-scale variability in soil properties [10]. Field observations therefore remain essential for establishing and validating SOC baselines, but they may provide insufficient spatial and temporal coverage when used alone [5,11].

These monitoring constraints have increased interest in combining field observations with spatially continuous environmental datasets. Satellite-derived vegetation indices and productivity products can provide information on vegetation dynamics and potential organic carbon inputs, while climate reanalysis datasets offer temporally consistent estimates of precipitation, temperature and evapotranspiration. Global digital soil mapping products can also provide estimates of SOC and clay content where local soil information is unavailable. However, these datasets differ substantially in their origin, spatial resolution and ability to represent local conditions. They should therefore be considered complementary to field observations rather than direct substitutes for site-specific measurements [5,12].

The integration of field observations, spatial datasets and process-based models is also increasingly relevant for monitoring, reporting and verification (MRV) frameworks. Such approaches can improve spatial coverage and reduce monitoring costs, but their reliability depends on the quality and representativeness of the underlying input data [13].

Process-based models provide a framework for integrating field observations and spatial environmental datasets to simulate long-term SOC dynamics. RothC (the Rothamsted Carbon Model) is designed to estimate SOC turnover in non-waterlogged soils, considering climate, soil texture, and organic inputs on a monthly basis. The model divides SOC into conceptual pools with different decomposition rates, allowing predictions of how carbon stocks will evolve under contrasting scenarios [14]. Recent applications have further extended RothC towards spatially explicit and hybrid modelling frameworks, combining process-based SOC simulations with satellite-derived indicators, gridded climate data and digital soil information to support regional carbon accounting and carbon farming assess-

ments [15–17]. This type of input-substitution approach is particularly relevant because recent RothC applications have shown that model outputs can be strongly affected by the estimation of carbon inputs, evapotranspiration, initial SOC stocks and soil-property layers, especially when spatial datasets are used instead of locally measured information [15,17,18].

The Guadiamar Green Corridor in southwestern Spain provides a particularly relevant case for evaluating SOC dynamics in a restored and heavily disturbed landscape. Following the 1998 Aznalcóllar mining spill, contaminated sludge was removed, substantial quantities of clay-rich mineral and organic amendments were applied, and the affected floodplain was progressively revegetated and transformed into a protected ecological corridor [19–21]. These interventions produced strongly modified soil conditions that may not be adequately represented by regional or global environmental datasets. The site therefore offers an opportunity to assess how field measurements and alternative environmental data sources influence long-term SOC simulations.

Despite the increasing integration of field observations, remote sensing, climate reanalysis and digital soil products in SOC modelling, their performance remains insufficiently evaluated in soils that have undergone abrupt anthropogenic disturbance and reconstruction [22,23]. In such environments, globally modelled soil properties may fail to capture the legacy of contamination, soil removal and amendment application [6,24]. Furthermore, errors in initial SOC stocks or other boundary conditions may propagate throughout the simulated period and lead to misleading interpretations of subsequent carbon dynamics [25].

The overarching aim of this study was to evaluate how alternative input datasets affect RothC simulations of long-term SOC dynamics in the Guadiamar Green Corridor. Specifically, the study aimed to: (i) quantify SOC changes observed between 2000, 2014 and 2024 in permanent monitoring plots representing riparian woodland, shrubland and grassland; (ii) compare a field-based reference configuration with boundary-condition scenarios in which selected soil and climate inputs were replaced by satellite-derived, climate-reanalysis and global soil datasets; (iii) identify the variables and land-cover types associated with the greatest model sensitivity; and (iv) implement a spatially explicit RothC simulation to evaluate landscape-scale SOC patterns and uncertainty. The purpose was not to assess whether alternative datasets can replace field measurements, but to assess the conditions under which they can complement field observations in data-scarce restored landscapes.

2. Materials and Methods

2.1. Study Area and Experimental Plots

The Guadiamar Green Corridor was established following the accidental mining tailings spill in Aznalcóllar on 25 April 1998, as an ecological recovery measure. Acid waters and sludge containing heavy metals from the tailings pond were discharged into the Agrio River and subsequently into the Guadiamar River. This event also caused both rivers to overflow, leading to widespread contamination of their floodplains [19,20]. The affected area covered 4286 ha, of which 2557 ha were agricultural lands [19,20].

The deposition of tailings on the soil not only introduced severe contamination from mining residues but also removed parts of the soil profile, reduced fertility, and altered its physical structure [26]. To remediate the affected soils, amendments were applied as an assisted natural remediation technique aimed at accelerating ecosystem recovery [6,20]. Inorganic amendments were used for arsenic stabilisation, while organic amendments were applied to restore soil fertility. Complementary techniques of phytoremediation and phytoextraction were also implemented [6,20,26].

The area is characterised by a Mediterranean climate, with mild, rainy winters (mean annual precipitation approximately 500 mm) and hot, dry summers. The mean annual daily temperature is around 17 °C, with a maximum of 33.5 °C in July and a minimum of 5.2 °C in January [26,27]. In the Guadiamar floodplain, soils generally present a neutral to slightly alkaline pH. However, lower pH values have been recorded in some terraces on the right bank, where clay contents are comparatively lower. Soil texture ranges from sandy loam to clay loam [27].

Six long-term monitoring plots were considered in this study (Figure 1). These plots were established between 1998 and 2000 as part of the post-spill monitoring network and were used as fixed landscape-monitoring units representing the main land-cover categories within the Guadiamar Green Corridor. The selected plots represented the main vegetation-cover types currently present in the study area: woodland (GUAD1, GUAD3 and GUAD6), shrubland (GUAD4 and GUAD5), and grassland (GUAD2). In this manuscript, the term "plot" refers to each of these six fixed landscape-monitoring units, while "soil replicates" refers to the individual soil samples collected within each plot during each sampling campaign.

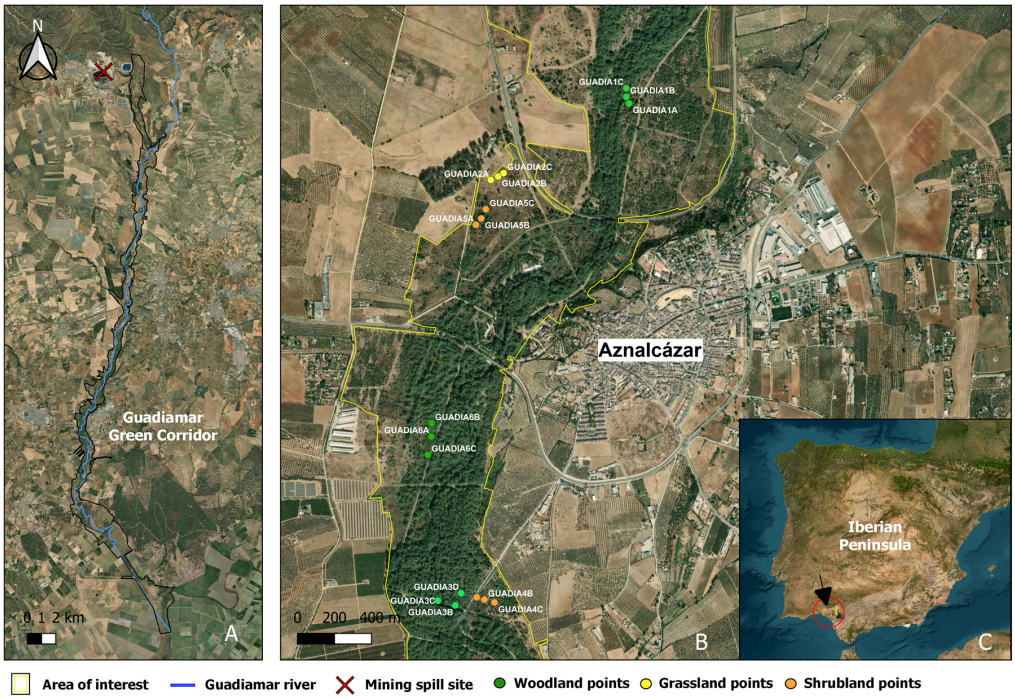

Figure 1. Guadiamar Green Corridor area of interest (AOI) composition. (**A**) The Guadiamar Green corridor Landscape level. (**B**) Sub-landscape level, showing the sampling points per land use. (**C**) The Iberian Peninsula and AOI location.

In the first sampling campaign (2000), five soil replicates were collected from each monitoring plot at two depths (0–15 cm and 15–30 cm), resulting in a total of 10 samples per plot. Replicates were spaced approximately 15–30 m apart, with the aim of capturing the internal spatial variability of each plot while maintaining consistency with the historical monitoring design. In the 2014 campaign, three replicates per plot were again collected at the same two depths. The 2024 sampling campaign was designed to reproduce, as closely as possible, the previous sampling locations using the georeferenced points from the 2000 and 2014 campaigns. In contrast to the previous campaigns, the 2024 sampling focused exclusively on the upper 0–20 cm soil layer, because the MRV4SOC campaign was designed to assess and validate SOC stocks in the topsoil layer most relevant for monitoring, reporting and verification purposes. Therefore, comparisons involving the

2024 campaign were interpreted as surface-layer SOC dynamics rather than as strictly equivalent full-profile comparisons with the 0–30 cm depth sampled in the 2000 and 2014 campaigns.

The higher number of replicates collected in 2000 was intended to capture the pronounced within-plot heterogeneity expected shortly after the remediation works. The monitoring design was therefore based on long-term georeferenced landscape units rather than on a fully balanced experimental design. Although several soil replicates were collected within GUAD2 during each sampling campaign, grassland was represented by only one independent monitoring plot. Consequently, the grassland results should be interpreted as a site-specific long-term case within the restored corridor and cannot be extrapolated to grassland areas across the wider region.

Prior to laboratory analysis, soil samples were air-dried, gently disaggregated and passed through a 2 mm sieve to separate the fine earth fraction from coarse fragments, roots and visible plant residues, following standard soil laboratory procedures as commonly recommended in soil survey protocols. SOC concentrations were determined using the Walkley–Black wet oxidation method [28]. Due to the application of organic–clay amendments and the dynamic nature of the soils, substantial differences were found in SOC contents, including abnormally high values compared with other Mediterranean Fluvisols [29]. Clay content was determined by particle-size analysis using the Boyoucos hydrometer method on field samples. Bulk density was determined using the undisturbed core method. For each soil layer, a known-volume metal cylinder was inserted into the soil, carefully extracted to preserve the soil structure, and transported to the laboratory (LABORATORIO AGRAMA C. Carmen Martín, 10, NAVE 11, 41300 Sevilla, Spain). The samples were oven-dried at 105 °C until constant weight, and bulk density was calculated as the ratio between the oven-dry soil mass and the volume of the cylinder. When visible roots, plant residues or coarse fragments were present, they were removed before weighing, and the corresponding correction was applied when coarse-fragment data were available. Soil organic carbon stocks were calculated from SOC concentration, bulk density and sampling depth according to the following equation:

$$SOC_{\text{stock}}\left(\text{Mg C ha}^{-1}\right) = SOC(\%) \times BD\left(\text{g cm}^{-3}\right) \times D\ (\text{cm})$$

For each study area, mean clay values were considered, since the application of amendments (such as red clays) altered soil granulometry in some zones of the study area, producing marked variability over short distances, like that observed in SOC concentrations.

2.2. RothC Configuration

In this study, we employed the RothC model (Rothamsted Carbon Model, version 26.3), developed by Rothamsted Research and described by Coleman and Jenkinson. The choice of RothC was based on several reasons: It requires a relatively small set of input data. It has been validated under a wide range of climatic and edaphic conditions, and it is widely used internationally for estimating SOC stocks, both in its original configuration and in adapted versions. In this case, the model was implemented in Rstudio 2023.06.0+421 using the SoilR package [15,30,31].

RothC partitions SOC into five conceptual compartments: decomposable plant material (DPM), resistant plant material (RPM), microbial biomass (BIO), humified organic matter (HUM), and one inert pool (IOM) [14,32]. Organic matter inputs to the soil are partitioned between DPM and RPM according to residue quality and land use. Carbon in these pools flows into BIO and HUM, with part being released as CO_2 through microbial decomposition processes. BIO and HUM also exchange carbon and release CO_2. Each active pool is characterised by a specific decomposition rate: DPM (0.165 years), RPM (2.31 years),

BIO (1.69 years), and HUM (49.5 years). The total CO_2 flux resulting from these processes can be compared with the monthly heterotrophic respiration of soils, providing an estimate of soil carbon turnover under varying climatic and management conditions [14,32].

RothC requires a set of essential parameters to initialise soil conditions and define the factors regulating carbon dynamics. Among these, the initial SOC content provides the baseline condition from which temporal SOC trajectories are simulated, while monthly carbon inputs, derived from plant residues (both above- and below-ground) or organic amendments such as manure or compost, represent the main source of decomposable organic matter [33]. Monthly climate variables, including precipitation, mean temperature, and potential evapotranspiration, further regulate microbial activity and thus the rate of carbon mineralisation [14,34]. Finally, clay content, expressed as weight percentage, plays a decisive role in SOC stabilisation, since higher fractions enhance its physical and chemical protection, thereby prolonging its persistence in the soil [35].

In the context of this study, several of these variables such as SOC, clay content, and climatic factors were obtained both from direct field measurements and from remote sensing products and statistical modelling. This combination enabled an evaluation, under the concept of boundary conditions, of the extent to which alternative input datasets can complement field measurements and support RothC simulations when local data are incomplete or unavailable, providing a framework applicable to contexts where field data availability is limited. For the execution of the model, eight different scenarios were defined, referred to as boundary conditions (BC), and labelled from BC0 to BC7. These scenarios were linked to the five key parameters considered in RothC: soil organic carbon, clay, precipitation, temperature, and evapotranspiration.

2.3. Input Data

RothC requires a range of soil, climate, and management input variables. Soil-related inputs include clay content (%), initial soil organic carbon stocks (t C ha^{-1}), and the initial distribution of carbon among the decomposable plant material (DPM), resistant plant material (RPM), microbial biomass (BIO), humified organic matter (HUM), and inert organic matter (IOM) pools. Climate inputs comprise monthly precipitation (mm), mean monthly air temperature (°C), and monthly open-pan evaporation or potential evapotranspiration (mm), depending on data availability and model configuration. Management inputs include carbon additions from plant residues, roots, rhizodeposition, and organic amendments (t C ha^{-1}), together with information on soil cover and the DPM/RPM ratio of the incoming organic material. The main soil and land-cover characteristics of the monitoring plots used to support model parameterisation are summarised in Table 1 meanwhile the set of minimum parameters for RothC is shown as Table 2.

The initial content of soil organic carbon (SOC) and clay was determined from sampling campaigns conducted in the study area between 1998 and 2000. To establish the baseline scenario, data from the year 2000 were used, collected only a few years after the restoration of the Guadiamar Green Corridor. The initial SOC stock and clay content used in the field-based reference configuration were derived from the 2000 sampling campaign, which was considered the baseline for the RothC simulations. SOC values were expressed as stocks after conversion from measured SOC concentrations using bulk density and sampling depth. The 2014 and 2024 field data were used for model evaluation. For each plot and campaign, SOC stock values were averaged across the available soil replicates before comparison with the corresponding RothC simulations. This approach was adopted due to the high variability in carbon content observed in this area because of organic amendment applications. Thus, for each study zone a single value was used, derived as the average of all collected samples.

Table 1. Soil and land-cover characteristics of the monitoring plots in 2024. Soil parameters correspond to mean values calculated from the soil replicates collected within each plot.

CODE	LULC	pH 1:5	Bulk Density (g/cm^3)	Sand (USDA %)	Silt (USDA %)	Clay (USDA %)	Main Species	Soil Class
GUAD1	Woodland	8.3	1.30	27.0	43.0	30.0	*Populus alba, Ulmus minor, Fraxinus angustifolia*	Fluvisols
GUAD2	Grassland	8.3	1.32	22.3	43.7	33.3	*Herbaceous plants*	Fluvisols
GUAD3	Woodland	8.3	1.29	21.0	44.3	33.0	*Populus alba, Ulmus minor, Fraxinus angustifolia*	Fluvisols
GUAD4	Shrubland	8.3	1.24	9.0	46.0	45.0	*Pistacia* sp., *Salix* sp., *Arbutus unedo*	Fluvisols
GUAD5	Shrubland	7.7	1.16	40.3	40.7	19.0	*Pistacia* sp., *Salix* sp., *Arbutus unedo*	Fluvisols
GUAD6	Woodland	8.3	1.28	18.7	46.3	35.0	*Populus alba, Ulmus minor, Fraxinus angustifolia*	Fluvisols

Table 2. Set of minimum parameters of RothC model.

Climate Data	Soil Data	Land-Use and Management Data
Monthly precipitation (mm)	Initial soil organic carbon stock at 0–30 cm depth (t C ha^{-1})	Monthly soil cover (binary: bare or vegetated)
Monthly mean air temperature (°C)	Initial carbon stocks in the RothC pools: DPM, RPM, BIO, HUM, and IOM (t C ha^{-1})	Monthly irrigation amounts added to precipitation (mm)
Monthly open-pan evaporation or potential evapotranspiration (mm)	Clay content (%)	Annual carbon inputs from plant residues, including aboveground biomass, roots, and rhizodeposition (t C ha^{-1} yr^{-1})
—	Soil depth (cm)	Annual carbon inputs from organic fertilisers and grazing-animal excreta (t C ha^{-1} yr^{-1})
—	—	DPM/RPM ratio, representing the relative decomposability of the incoming plant material

Annual carbon inputs represent the continuous incorporation of organic matter into the soil, either in the form of plant residues (both aboveground biomass and roots) or organic amendments such as manure or compost. As direct records were not available for the entire study period, these inputs were estimated by combining land-cover data, residue production coefficients reported in the literature for each vegetation type, and assumptions about the proportion of biomass returned to the soil after the production cycle. To obtain realistic estimates of the annual carbon inputs required by the RothC model, an empirical approach was adopted that integrates vegetation dynamics observed through remote sensing with eco-physiological parameters drawn from the literature.

For each land use type (grassland, shrubland, and woodland), mean annual NDVI values were calculated from Landsat imagery (2000–2024), as shown in Figure 2. These values were then converted into the fraction of absorbed photosynthetically active radiation (fPAR) using the widely applied linear relationship fPAR = 1.24·NDVI—0.168 [36]. Absorbed

photosynthetically active radiation (APAR) was derived by multiplying fPAR by local estimates of incident annual photosynthetically active radiation (≈2000 MJ m^{-2} yr^{-1} in southern Spain) [37]. Net primary productivity (NPP) was then estimated as the product of APAR and light use efficiency (ε), using ecosystem-specific values reported in the literature: 0.85 g C MJ^{-1} for grasslands [38], 0.65 g C MJ^{-1} for Mediterranean shrublands [37,39], and 0.95 g C MJ^{-1} for riparian forests [40].

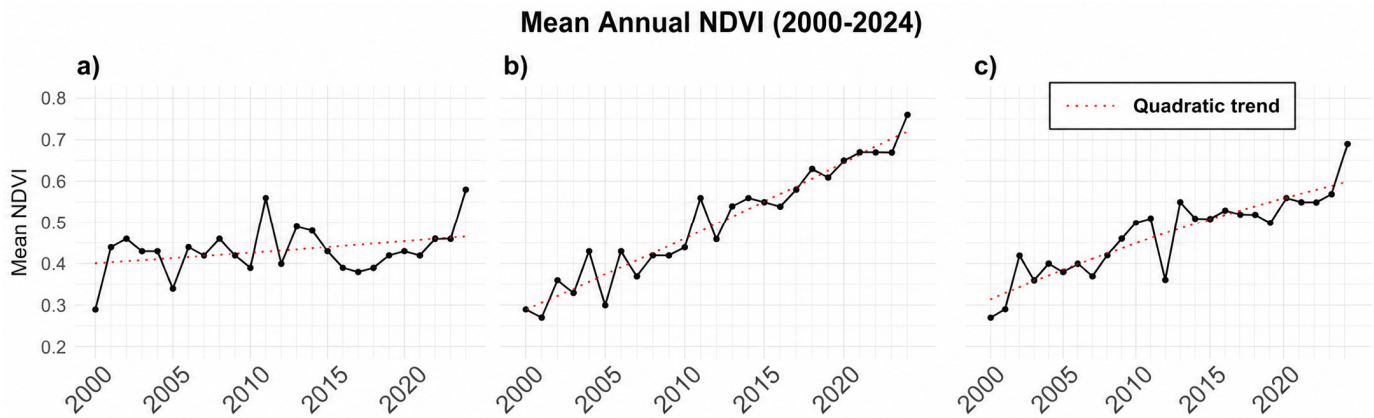

Figure 2. Mean annual NDVI values derived from Landsat imagery for the land-cover categories represented by the monitoring plots during 2000–2024: (**a**) grassland, (**b**) woodland and (**c**) shrubland.

To approximate the fraction of NPP returning to the soil via roots, litterfall, and below-ground detritus, specific allocation coefficients (fsoil) were applied: 0.40 for grasslands, reflecting their high root turnover and herbaceous inputs; 0.25–0.30 for shrublands, consistent with their woodier and more recalcitrant biomass; and 0.15–0.20 for riparian forests, where a large share of NPP accumulates in persistent tissues [41]. These coefficients were further adjusted to reflect Mediterranean eco-physiological constraints such as summer drought and seasonal growth pulses. Finally, the fractions of rapidly decomposable and resistant materials were parameterised in RothC using the recommended DPM/RPM ratios for each land use (DR = 1.44 for improved grasslands, 0.67 for shrublands or unimproved grasslands, and 0.25 for forests), reflecting differences in residue quality and lignin content [14]. This procedure yielded coherent, literature-based estimates of annual carbon inputs (t C ha^{-1} yr^{-1}), which were subsequently used to drive RothC simulations of soil organic carbon dynamics under different land-use scenarios.

Climatic information on precipitation, temperature, and monthly evaporation in situ was obtained from the Aznalcázar meteorological station, located at 37°09′06″ N, 06°16′24″ W, at an elevation of 2 metres above sea level. This database provided continuous records from October 2000 to February 2025. In parallel, to obtain gridded precipitation, temperature and evaporation estimates from climate reanalysis, a script was implemented in the Google Earth Engine (GEE) processing environment. The ERA5-Land dataset [42] was employed, which is a high-resolution climate reanalysis product developed by the European Centre for Medium-Range Weather Forecasts (ECMWF) within the framework of the Copernicus Climate Change Service (C3S). This dataset is available from 1950 onwards, with a spatial resolution of approximately 9 km and a monthly temporal frequency. The selected variables were extracted and processed through GEE for the study period.

Finally, since radiocarbon measurements and SOC stock pools were not available, the RothC model was initialised through a spin-up procedure using the SoilR implementation. First, the monthly environmental modifier (ξ) was calculated from temperature (fT), water balance (fW; soil depth of 20 cm, pClay), and a constant cover factor (fC = 0.6), under the long-term mean climate. Subsequently, a function was used to derive an equilibrium

allocation of the observed initial SOC stock across the DPM, RPM, BIO, HUM, and IOM compartments, assuming the following respective litter quality ratios for forest, shrubland, and grassland: DR = 0.25, DR = 0.67, and DR = 1.44. The IOM compartment was not prescribed using a pedotransfer function but emerged from the equilibrium solution. This procedure also provided a baseline carbon input (≈2.20 Mg C ha^{-1} yr^{-1}), which was then used as a reference for transient simulations, with time-varying inputs derived from the litter table.

2.4. Model Spin-Up Initialization

Before running the RothC simulations, a spin-up procedure was applied to initialise the distribution of SOC among the model pools. This step was necessary because direct measurements of the different RothC carbon compartments were not available for the study area. The spin-up was implemented using the SoilR package in R, following the RothC model structure. For each land-cover type, the observed initial SOC stock from the baseline sampling period was used as the target SOC value. The model was then run under long-term mean climatic conditions until an equilibrium state was reached. Monthly environmental modifiers were calculated from temperature, soil moisture and vegetation cover effects. The soil moisture modifier was estimated using monthly precipitation and evapotranspiration data, soil depth and clay content, while a constant vegetation cover factor was applied to represent the protective effect of plant cover on decomposition. The quality of organic inputs was defined through land-cover-specific DPM/RPM ratios. A ratio of 0.25 was used for forested areas, 0.67 for shrubland, and 1.44 for grassland, reflecting differences in residue decomposability and lignin content. These ratios determined the allocation of fresh organic matter inputs between the fast-cycling and more resistant plant material pools.

The spin-up procedure allowed the model to derive an internally consistent initial allocation of SOC across the RothC pools. This ensured that the baseline SOC stock used in the simulations was compatible with local climate, soil texture and land-cover conditions. The resulting pool distribution was subsequently used as the initial condition for the transient simulations covering the 2000–2024 period. In this way, the spin-up reduced the uncertainty associated with unknown initial pool sizes and provided a stable starting point for comparing the different boundary condition scenarios.

2.5. Sub-Landscape Analysis Using Boundary Conditions Scenarios (BC0–BC7)

To evaluate the performance of the RothC model in simulating soil organic carbon (SOC) dynamics in the monitoring plots of Guadiamar Green Corridor, a boundary condition-based approach was implemented (Table 3) across the three main land-use types considered in this study: grassland, shrubland and woodland. Boundary conditions (BCs) were defined as alternative model-input configurations in which specific field-derived variables were replaced by values obtained from satellite-derived products, climate reanalysis datasets or global soil databases. This approach allowed us to assess the extent to which non-field-based data sources can be used to support SOC modelling and monitoring, reporting and verification (MRV) methodologies under different levels of data availability.

The analysis started with the reference scenario, BC0, in which all RothC input variables were derived from field measurements or local meteorological records, with the exception of carbon inputs. Since direct records of annual carbon inputs were not available for the whole study period, this variable was estimated from vegetation dynamics using NDVI-derived proxies, as described in the previous section. BC0 was therefore considered the closest approximation to an in situ-based modelling configuration and was used as the baseline scenario against which the remaining boundary conditions were compared. BC1

was designed to evaluate the effect of replacing the initial SOC stock with values derived from SoilGrids. In this scenario, the baseline SOC used to initialise the RothC model was obtained from global soil information rather than from field observations, while the remaining variables were kept consistent with the reference configuration. This scenario was included to assess whether globally available SOC datasets can provide a reliable alternative for RothC initialisation in areas where field measurements are scarce or unavailable. BC2 assessed the influence of replacing clay content with SoilsGrids values. Clay is a key parameter in RothC because it influences the stabilisation of organic carbon and the partitioning of decomposed material between CO_2, microbial biomass and humified organic matter. Therefore, this scenario allowed us to test the sensitivity of SOC dynamics to modelled soil texture information. BC3 to BC6 focused on the substitution of climatic variables. In BC3, precipitation data were replaced by remote sensing or reanalysis-derived estimates; in BC4, air temperature was substituted; and in BC5, evapotranspiration was replaced. BC6 combined the substitution of all climatic variables, providing an integrated assessment of the effect of using remote sensing-based climate inputs instead of local meteorological station records. These scenarios were used to evaluate the suitability of open-access climate datasets for driving RothC simulations in contexts where long-term local climatic records are incomplete or unavailable. Finally, BC7 evaluated the effect of replacing all selected field-derived inputs with alternative open-access datasets.

Table 3. Boundary-condition scenarios used to evaluate the replacement of field-derived RothC inputs with alternative open-access datasets.

Model	Baseline C	Clay	Climate	C input
BC0	Init C	Clay	Climate	**C input**
BC1	**Init C**	Clay	Climate	**C input**
BC2	Init C	**Clay**	Climate	**C input**
BC3	Init C	Clay	**Climate (Prec)**	**C input**
BC4	Init C	Clay	**Climate (Temp)**	**C input**
BC5	Init C	Clay	**Climate (Evap)**	**C input**
BC6	Init C	Clay	**All Climate**	**C input**
BC7	**Init C**	**Clay**	**Climate**	**C input**

2.6. Landscape Analysis

2.6.1. Data Acquisition and Spatiotemporal Structuring

Baseline soil organic carbon stocks (SOC_0) and soil clay content (%) were obtained from the SoilGrids and OpenLandMap global datasets at a 250 m spatial resolution. Monthly hydrometeorological forcing data (air temperature, precipitation, and potential evapotranspiration) were extracted from the ECMWF ERA5-Land reanalysis dataset for the 2000–2024 period. Annual soil carbon inputs (C_{input}) were estimated using Net Primary Productivity (NPP) products from the MODIS sensor (MOD17A3HGF). All spatial layers were reprojected to the UTM Zone 31N coordinate reference system (EPSG:32631) and bilinearly resampled to the 250 m reference grid. To optimize computational efficiency, the spatial domain was vectorized into a 2D spatiotemporal matrix $\left(N_{\text{pixels}} \times 300\,\text{months}\right)$. Because the satellite-derived NPP data were annual, carbon inputs were temporally disaggregated into monthly intervals using an empirical weighting vector derived from Mediterranean ecosystem litterfall dynamics $(w = [3.8,\ 6.9,\ 4.7,\ 2.7,\ 5.6,\ 6.6,\ 5.7,\ 11.7,\ 12.3,\ 24.7,\ 10.8,\ 4.2]$ from January to December, capturing the characteristic autumn litterfall peak.

2.6.2. Model Parameterization, Spin-Up, and Transient Simulation

The RothC model was parameterized with a soil depth profile of 20 cm, a land-cover factor (f_c) of 0.6, zero external farmyard manure additions $(FYM = 0)$ and a decomposable-to-resistant plant material (DPM/RPM) ratio of 0.2 (representing 17% decomposable and 83% resistant biomass). Default specific decomposition rates at 20 °C were retained (10.0, 0.3, 0.66, and 0.02 yr^{-1} for the DPM, RPM, BIO, and HUM pools, respectively). To establish thermodynamic equilibrium between the active carbon pools and local edaphoclimatic conditions, an analytical spin-up procedure was performed. Steady-state initial carbon compartments (C_0) were resolved via matrix inversion using the SoilR R package, driven by the 2000–2010 baseline climatology. Following spin-up equilibrium, pixel-by-pixel transient simulations were executed dynamically across the 2000–2024 historical period. At each monthly time step, carbon pool stocks were updated based on local temperature and soil moisture rate-modifying factors. From the resulting spatiotemporal matrix, annual SOC stock rasters were extracted for each modelled year, alongside a final spatial map of net cumulative SOC stock changes $(\Delta SOC = SOC_{2024} - SOC_{2000})$, expressed in $\left(\mathrm{t\,C \cdot ha^{-1}}\right)$.

2.6.3. Spatial Uncertainty Propagation and Raster Outputs

To account for landscape heterogeneity and input data uncertainty, a spatially explicit bounding scenario framework was implemented. For each valid grid cell, upper and lower simulation bounds were calculated by simultaneously perturbing annual carbon inputs (C_{input}) and the decomposition rate modifier (DR) by 20. This yielded a conservative lower-bound scenario $(C_{\mathrm{input}} \times 0.8, DR \times 0.8)$ and an optimistic upper-bound scenario $(C_{\mathrm{input}} \times 1.2, DR \times 1.2)$. Based on these bounding runs, spatial uncertainty metrics were derived for the final year (2024), mapping the 5th and 95th carbon stock percentiles $(SOC_{\mathrm{p05}}\ and\ SOC_{\mathrm{p95}})$, the absolute uncertainty range $(SOC_{\mathrm{p95}} - SOC_{\mathrm{p05}})$, and the relative spatial uncertainty via the Prediction Interval Ratio $(PIR = [SOC_{\mathrm{p95}} - SOC_{\mathrm{p05}}]/SOC_{2024})$. The workflow yielded a high-resolution GeoTIFF database comprising monthly and annual SOC time-series raster stacks, baseline and final SOC inventories, the cumulative ΔSOC balance map, and the comprehensive suite of spatial uncertainty layers.

3. Results

3.1. Observed SOC Changes in the Monitoring Plots

Observed soil organic carbon stocks varied substantially among monitoring plots and sampling campaigns (Table 4). At the beginning of the monitoring period, SOC stocks ranged from 51.75 Mg C ha^{-1} at the grassland plot GUAD2 to 83.81 Mg C ha^{-1} at the shrubland plot GUAD4. The woodland plots showed intermediate initial values, ranging from 55.31 Mg C ha^{-1} at GUAD1 to 70.88 Mg C ha^{-1} at GUAD3.

Table 4. Mean SOC stock and standard deviation for each monitoring plot and sampling campaign.

Sampling Site	Land Use	2000 Mean SOC Stock (t C/ha)	2000 STD ± (t C/ha)	2014 Mean SOC Stock (t C/ha)	2014 STD ± (t C/ha)	2024 Mean SOC Stock (t C/ha)	2024 STD ± (t C/ha)
GUAD1	Woodland	55.31	22.00	59.44	2.9	16.69	6.3
GUAD2	Grassland	51.75	10.17	57.94	7.97	19.56	12.9
GUAD3	Woodland	70.88	28.63	63.19	5.31	42.38	5.9
GUAD4	Shrubland	83.81	9.23	60.94	4.13	30.81	1.27
GUAD5	Shrubland	69.19	11.13	55.88	9.61	16.81	3.6
GUAD6	Woodland	60.38	26.55	46.69	4.37	41.94	10.9

Between 2000 and 2014, the direction and magnitude of SOC change differed among plots. SOC increased moderately at GUAD1, from 55.31 to 59.44 Mg C ha^{-1}, and at GUAD2, from 51.75 to 57.94 Mg C ha^{-1}. In contrast, SOC declined at the remaining four plots. The largest decrease during this first period was observed at GUAD4, where SOC fell by 22.87 Mg C ha^{-1}, followed by GUAD6 and GUAD5, with decreases of 13.69 and 13.31 Mg C ha^{-1}, respectively. GUAD3 showed a smaller reduction of 7.69 Mg C ha^{-1}. A general decline was observed between 2014 and 2024 across all six monitoring plots. The greatest decreases occurred at GUAD1, GUAD2 and GUAD5, where SOC stocks declined by 42.75, 38.38 and 39.07 Mg C ha^{-1}, respectively. GUAD4 and GUAD3 showed decreases of 30.13 and 20.81 Mg C ha^{-1}, whereas GUAD6 showed the smallest change during this period, declining by 4.75 Mg C ha^{-1}.

Over the complete 2000–2024 period, all monitoring plots showed lower SOC stocks in the final campaign than at baseline. The largest absolute declines were recorded in the shrubland plots GUAD4 and GUAD5, with reductions of 53.00 and 52.38 Mg C ha^{-1}, respectively. Woodland plots showed more variable trajectories, with total reductions of 38.62 Mg C ha^{-1} at GUAD1, 28.50 Mg C ha^{-1} at GUAD3 and 18.44 Mg C ha^{-1} at GUAD6. At the single grassland plot, GUAD2, SOC declined by 32.19 Mg C ha^{-1} between 2000 and 2024.

Within-plot variability also differed among sampling campaigns. The largest standard deviations were generally observed in the 2000 campaign, particularly at GUAD3 and GUAD6, indicating substantial initial spatial heterogeneity within these monitoring units. Lower standard deviations were generally recorded in 2014 and 2024, although variability remained comparatively high at GUAD2 and GUAD6 in the final campaign. These differences should be interpreted cautiously because the number of soil replicates differed among sampling years.

Overall, the field observations suggest a dominant reduction in surface-layer SOC stocks, particularly after 2014. The largest losses were observed in the two shrubland plots, whereas the woodland plots displayed more heterogeneous trajectories. Results for grassland represent only the site-specific behaviour of GUAD2, because this land-cover category was represented by a single independent monitoring plot and cannot be extrapolated to other grassland areas within the region.

3.2. Model Performance Across Land-Cover Categories

Model performance differed among the three land-cover categories when the results were aggregated across all evaluated input configurations (Table 5). Overall, woodland showed the closest agreement between observed and simulated SOC stocks, whereas shrubland presented the highest average errors and the greatest variability in model performance. The grassland results showed an intermediate level of agreement, although they represent only the site-specific response of the single grassland monitoring plot, GUAD2.

Table 5. Mean performance per land use.

Land Use	Mean RMSE	Mean EF	Mean d (Willmott)	Mean PBIAS (%)	Mean Bias
Woodland	8.62	0.487	0.802	+0.04	0.02
Grassland	14.90	0.208	0.616	−5.61	−2.42
Shrubland	18.79	0.213	0.712	+10.45	5.53

Woodland showed the best overall model performance, with the lowest mean RMSE (8.62 Mg C ha^{-1}), the highest mean Nash–Sutcliffe efficiency (EF = 0.487) and the highest mean Willmott agreement index (d = 0.802). Both mean PBIAS (+0.04%) and mean bias (+0.02 Mg C ha^{-1}) were close to zero, indicating that the simulations showed little sys-

tematic deviation from the observed SOC stocks when the different input configurations were considered together. Woodland also showed the most consistent performance across configurations, with RMSE values ranging from 7.26 to 13.52 Mg C ha^{-1}.

The single grassland monitoring plot, GUAD2, showed a higher mean RMSE than the woodland category (14.90 Mg C ha^{-1}), together with lower mean EF and Willmott agreement values of 0.208 and 0.616, respectively. Mean PBIAS (−5.61%) and mean bias (−2.42 Mg C ha^{-1}) indicated a moderate overall tendency towards lower simulated than observed SOC stocks under the sign convention adopted in this study. RMSE values ranged from 14.29 to 18.69 Mg C ha^{-1}. However, because grassland was represented by only one independent monitoring plot, these metrics describe model behaviour specifically at GUAD2 and cannot be extrapolated to other grassland areas within the Guadiamar Green Corridor or the wider region.

Shrubland showed the highest mean RMSE among the evaluated land-cover categories (18.79 Mg C ha^{-1}). Its mean EF was 0.213, similar to that obtained for the grassland plot, whereas its mean Willmott agreement index was higher (d = 0.712). Mean PBIAS (+10.45%) and mean bias (+5.53 Mg C ha^{-1}) indicated an overall tendency towards higher simulated than observed SOC stocks. Shrubland also showed the widest variation in RMSE, ranging from 14.86 to 31.20 Mg C ha^{-1}, indicating that model performance was less consistent for this category than for woodland or the grassland plot.

In summary, woodland showed the most accurate and consistent model performance across the evaluated input configurations, as indicated by its lower errors, higher agreement metrics and minimal systematic bias. Shrubland showed the greatest average error and the highest variability, whereas the grassland plot presented intermediate performance. The influence of the individual input configurations on these land-cover-specific differences is examined separately in Section 3.3.

3.3. Sensitivity to Boundary-Condition Scenarios

Model performance varied according to the input variables replaced in each boundary-condition scenario (Table 6 and Figure 3). Overall, the replacement of the initial SOC stock produced the largest deterioration in model performance, whereas the use of alternative climate data generally maintained or improved agreement with the field observations.

Table 6. Results from the model performance analysis per land use and boundary conditions.

BC	Land Use	RMSE	EF (Nash–Sutcliffe)	d (Willmott)	PBIAS (%)	Mean Bias
BC0	Woodland	8.26	0.550	0.796	+4.8%	2.42
BC0	Grassland	14.30	0.278	0.600	−0.9%	−0.37
BC0	Shrubland	17.78	0.339	0.717	+20.4%	10.79
BC1	Woodland	13.52	−0.205	0.649	−20.1%	−10.20
BC1	Grassland	18.69	−0.235	0.586	−26.5%	−11.44
BC1	Shrubland	31.20	−1.037	0.533	−47.3%	−25.04
BC2	Woodland	8.14	0.563	0.806	+4.3%	2.17
BC2	Grassland	14.30	0.278	0.598	−0.8%	−0.32
BC2	Shrubland	17.92	0.328	0.712	+20.5%	10.85
BC3	Woodland	8.06	0.571	0.813	+3.8%	1.91
BC3	Grassland	14.35	0.273	0.604	−1.3%	−0.57
BC3	Shrubland	17.52	0.358	0.722	+19.8%	10.46
BC4	Woodland	7.91	0.587	0.823	+3.4%	1.74
BC4	Grassland	14.29	0.278	0.614	−1.7%	−0.73
BC4	Shrubland	17.52	0.358	0.720	+19.7%	10.44

Table 6. *Cont.*

BC	Land Use	RMSE	EF (Nash–Sutcliffe)	d (Willmott)	PBIAS (%)	Mean Bias
BC5	Woodland	7.48	0.632	0.863	+0.1%	0.08
BC5	Grassland	14.50	0.258	0.653	−5.1%	−2.22
BC5	Shrubland	15.71	0.484	0.774	+15.9%	8.42
BC6	Woodland	7.26	0.652	0.877	−0.9%	−0.46
BC6	Grassland	14.46	0.261	0.671	−6.4%	−2.76
BC6	Shrubland	14.86	0.538	0.803	+14.3%	7.58
BC7	Woodland	8.32	0.544	0.789	+4.9%	2.49
BC7	Grassland	14.34	0.273	0.603	−2.2%	−0.94
BC7	Shrubland	17.79	0.338	0.715	+20.3%	10.73

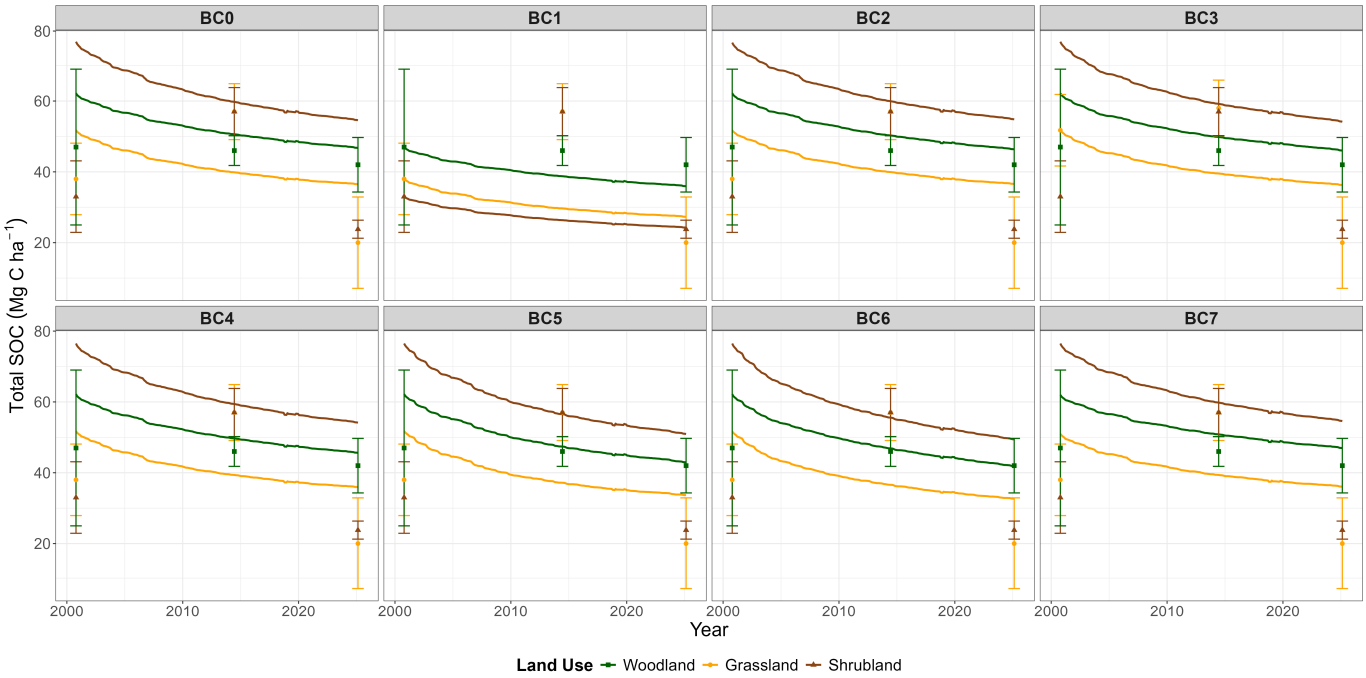

Figure 3. Carbon dynamics of each BC scenario. Yellow—Grassland land use; Green—Woodland use; Red—Shrubland use. BC0 (in situ variables), BC1 (SOC SoilsGrid), BC2 (clay SoilsGrid), BC3 (precipitation), BC4 (temperature), BC5 (ETP), BC6 (all climatic variables), BC7 (all RS variables).

BC1 showed the poorest performance across all land-cover categories. Replacing the initial SOC stock increased RMSE to 13.52 Mg C ha^{-1} in woodland, 18.69 Mg C ha^{-1} in the grassland plot and 31.20 Mg C ha^{-1} in shrubland. EF values were negative in all three categories, while PBIAS ranged from −20.1% to −47.3%, indicating systematic underestimation of observed SOC stocks. These results demonstrate the strong sensitivity of RothC to the SOC baseline used for model initialisation.

The substitution of clay content in BC2 and of precipitation or temperature in BC3 and BC4 produced relatively small changes compared with the reference configuration, BC0. Their performance metrics remained broadly similar across land-cover categories, indicating a lower model sensitivity to these individual substitutions.

Replacing evapotranspiration in BC5 improved model performance, particularly in woodland and shrubland. BC6, in which all climate variables were replaced simultaneously, provided the most consistent overall performance. It produced the lowest RMSE in woodland and shrubland—7.26 and 14.86 Mg C ha^{-1}, respectively—and the highest EF and Willmott agreement values for these categories. In the grassland plot, BC6 produced the highest Willmott agreement index (d = 0.671), although its RMSE was slightly higher

than that obtained under BC4. BC7 showed results broadly similar to the reference configuration and did not retain the improvements observed when only the climate variables were replaced.

The simulated trajectories in Figure 3 were consistent with the statistical metrics. BC5 and BC6 generally followed the observed SOC dynamics more closely, whereas BC1 showed the largest and most persistent deviation from the field observations. Overall, the results indicate that RothC was more sensitive to the initial SOC dataset than to the replacement of clay or individual climate variables, while BC6 showed the most consistent statistical performance among the evaluated boundary-condition scenarios.

3.4. Landscape-Scale SOC Dynamics

Across the 1008 valid 250 m grid cells, mean simulated SOC stock increased from 22.68 Mg C ha^{-1} in 2000 to 25.45 Mg C ha^{-1} in 2024 (Figure 4). This represented a mean net change of 2.77 ± 2.62 Mg C ha^{-1}. SOC gains occurred in 85.02% of the modelled area (857 grid cells), with a mean increase of 3.59 Mg C ha^{-1} and a maximum simulated gain of 10.21 Mg C ha^{-1}. SOC losses occurred in the remaining 14.98% of the area (151 grid cells), with a mean decrease of 1.86 Mg C ha^{-1} and a maximum simulated loss of 6.42 Mg C ha^{-1}.

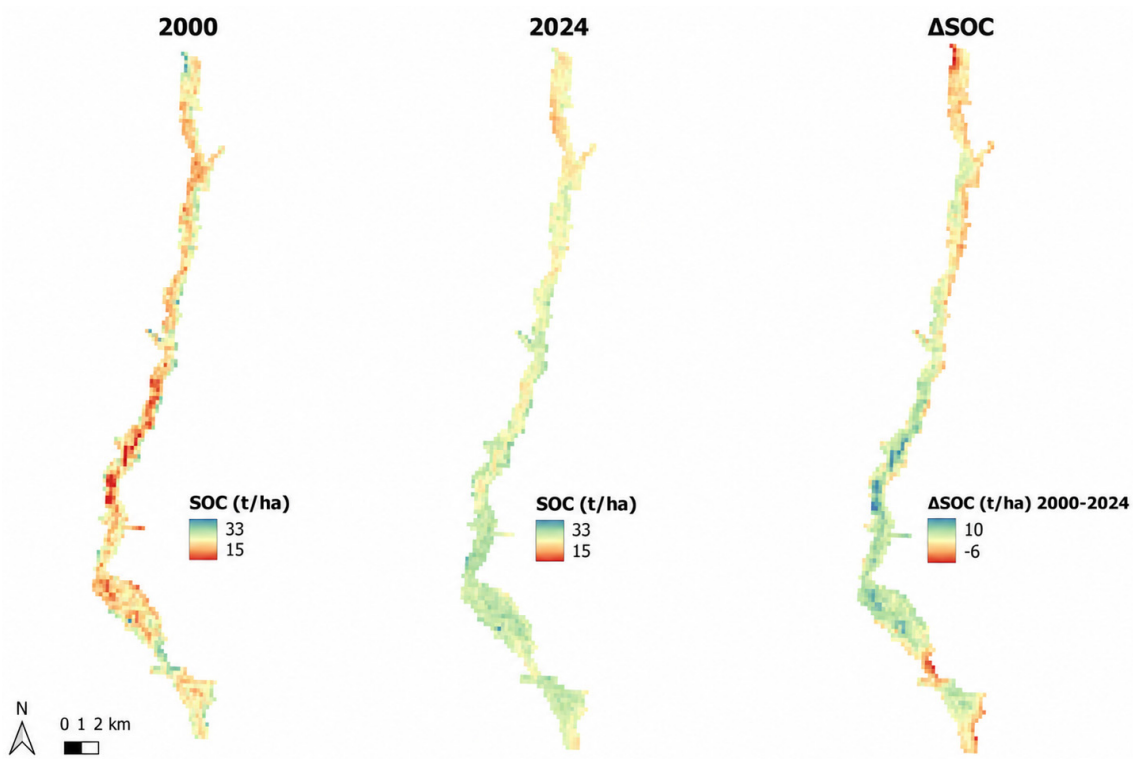

Figure 4. Landscape-scale simulated SOC stocks in 2000 and 2024, and simulated SOC change between 2000 and 2024 across the Guadiamar Green Corridor. SOC maps for 2000 and 2024 use the same colour scale to allow direct comparison, while ΔSOC is displayed using a separate scale centred on zero.

Simulated SOC change was positively correlated with mean annual MODIS-derived carbon inputs (r = 0.743). Grid cells acting as carbon sinks received mean annual inputs of 3.48 Mg C ha^{-1} yr^{-1}, compared with 2.89 Mg C ha^{-1} yr^{-1} in cells acting as carbon sources. SOC change was also negatively correlated with the initial SOC stock (r = −0.797). Cells showing net SOC losses had higher mean baseline stocks (26.34 Mg C ha^{-1}) than cells showing net gains (22.03 Mg C ha^{-1}).

Overall, the spatial simulation indicated that SOC trajectories were associated with both the magnitude of organic carbon inputs and the initial SOC conditions.

3.5. Spatial Uncertainty

The bounding-scenario analysis, based on ±20% perturbations in annual carbon inputs and decomposition-rate modifiers, produced a mean relative uncertainty of 11.28% across the modelled area, with spatial values ranging from approximately 7% to 14% (Figure 5). The lower-bound simulation retained a positive mean regional SOC balance, indicating that the overall simulated increase remained positive under the conservative input configuration.

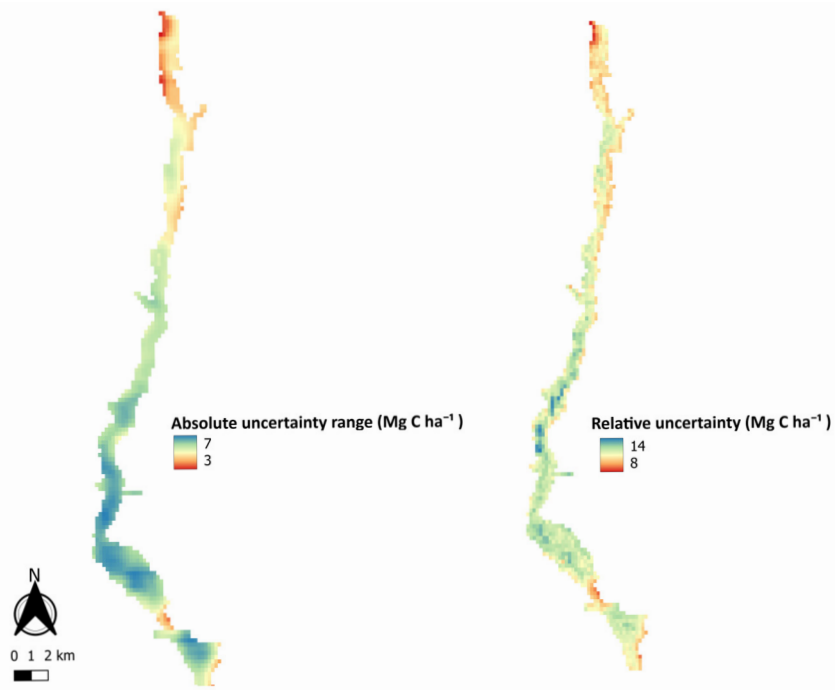

Figure 5. Spatial distribution of uncertainty in simulated SOC stocks across the Guadiamar Green Corridor: (**Left**) absolute uncertainty range and (**Right**) relative uncertainty. Uncertainty was estimated using lower- and upper-bound scenarios based on ±20% perturbations in annual carbon inputs and decomposition-rate modifiers.

Across the 1008 valid grid cells, the Prediction Interval Ratio (PIR) had a mean value of 0.226, equivalent to 22.56% of the central SOC estimate. The interquartile range extended from 0.213 to 0.238, while values across the full modelled area ranged from 0.156 to 0.280. Spatial uncertainty was therefore relatively homogeneous, although higher PIR values occurred in areas showing greater sensitivity to the perturbed input parameters. PIR was strongly correlated with the absolute magnitude of simulated SOC change (r = 0.991), indicating that grid cells with larger simulated gains or losses also showed wider uncertainty intervals. Overall, the uncertainty analysis showed that the magnitude of local SOC change was more sensitive to input perturbations than the direction of the mean regional carbon balance.

4. Discussion

4.1. Sub-Landscape

Among the evaluated land-cover categories, riparian woodland showed the most consistent agreement between observed and simulated SOC stocks. A plausible explanation is that the combined effects of canopy cover, forest-floor litter and root systems reduce short-term hydrothermal variability and provide comparatively regular organic carbon inputs [40]. Forest canopies buffer temperature extremes and modify near-surface moisture conditions, while the litter layer protects the mineral soil and supplies carbon through grad-

ual decomposition. Fine-root turnover, rhizodeposition and root exudates also introduce carbon directly into the soil, where part of it may contribute to particulate or mineral-associated organic matter [43,44]. These comparatively buffered environmental conditions and more continuous above- and below-ground inputs may be better represented by RothC's monthly temperature and moisture modifiers and its pool-based treatment of organic matter than the more episodic and spatially heterogeneous conditions found in shrubland and grassland. However, canopy microclimate, litter stocks and root dynamics were not measured directly in this study; therefore, these mechanisms should be interpreted as literature-supported explanations rather than demonstrated causal relationships.

In contrast, grassland and shrubland formations presented intermediate to high modelling uncertainty, accompanied by lower efficiency coefficients. In Mediterranean grasslands, carbon turnover is inherently dynamic and subject to pronounced interannual climatic fluctuations. The high allocation of net primary productivity to fine roots and easily decomposable herbaceous tissues makes grassland topsoils highly responsive to seasonal precipitation pulses and summer drought dormancy [38]. However, the interpretation of grassland model performance requires additional caution because this land-cover class was represented by a single long-term monitoring plot. Therefore, the grassland results provide useful information on model behaviour under herbaceous vegetation within the Guadiamar restoration context, but they should not be interpreted as a fully replicated assessment of grassland SOC dynamics at landscape scale. In shrublands, the observed temporal dispersion stems from the extreme spatial heterogeneity of vegetation colonization and structural patchiness following the post-mining restoration. Patchy shrub canopies generate highly localized islands of fertility separated by bare or sparsely vegetated soil, resulting in high micro-scale variability in field SOC measurements that a 1D point-based simulation cannot fully capture without high-resolution spatial aggregation.

The progressive substitution of in situ observations with remote sensing and reanalysis datasets (the boundary condition framework, BC0–BC7) provided critical insights into the operational feasibility and sensitivity of process-based soil organic carbon (SOC) modelling in restoration contexts. A notable finding of this study was the comparatively strong performance of scenario BC6, where local meteorological station records of temperature, precipitation, and evapotranspiration were entirely replaced by the ERA5-Land reanalysis dataset. Across all evaluated land uses, most notably in woodland formations $\left(\mathrm{RMSE} = 7.26\ \mathrm{Mg\ C \cdot ha^{-1}}, \mathrm{EF} = 0.65\right)$, the BC6 configuration matched or even slightly exceeded the predictive accuracy of the in situ reference scenario (BC0).

A notable pattern identified in the sub-landscape simulations was the widespread decline in SOC stocks across several monitoring plots in soil organic carbon (SOC) stocks observed across several monitoring plots over the 25-year timeframe. Rather than indicating an ecosystem degradation process, this downward trajectory may reflect a post-remediation adjustment phase towards a new soil carbon equilibrium. The initial soil inventories measured in 2000 were strongly influenced by the substantial application of organic-clay amendments implemented as an emergency remediation strategy to immobilize heavy metals and reconstruct the topsoil profile immediately after the 1998 Aznalcóllar mine spill [6]. These baseline inventories far exceed the natural carrying capacity of typical Mediterranean Fluvisols under dryland conditions, which baseline models and empirical regional studies estimate to range between 20 and 35 [29,45]. Once the active external organic inputs ceased, the highly active microbial pools simulated in RothC rapidly mineralized the labile fractions of these exogenous amendments. Crucially, only the riparian forest (woodland) formations possessed high net primary productivity (NPP), stable litterfall inputs, and buffered microclimatic moisture conditions necessary to physically protect and sustain these elevated carbon stocks. In contrast, the water-limited grasslands and shrublands,

subjected to intense Mediterranean summer drought and lower organic return rates, could not support the amended carbon inventories, triggering a steep transient decay toward their true biogeochemical carrying capacity.

This initial anthropogenic distortion was further compounded by extreme micro-spatial heterogeneity within the experimental plots, as evidenced by the exceptionally high standard deviations (STD) recorded among sampling replicates during the baseline campaign in the year 2000. In these early post-remediation stages, the spatial variance reached critical magnitudes relative to the plot means. This was most notable in woodland plots where the standard deviation represented nearly 40% to 45% of the total carbon stock. This massive spatial noise serves as a direct diagnostic signature of the highly uneven, mechanically patchy application of composted amendments and red clays during the emergency soil reconstruction phase [26]. Over the 25-year chronosequence, however, this early spatial heterogeneity experienced a highly pronounced natural stabilization and homogenization. By 2014 and 2024, the standard deviations between replicates dropped dramatically across almost all monitoring plots. This long-term spatial stabilization reflects the gradual biogeochemical integration of the exogenously added organic matter through continuous root expansion, macro-invertebrate bioturbation, and localized microbial mineralization of carbon hotspots [27]. These findings confirm that while empirical baseline inventories in reconstructed soils are highly vulnerable to micro-scale spatial noise, natural soil development processes act as spatial homogenizers over multi-decadal scales, gradually reconciling local field inventories with regional baseline projections.

These contrasting outcomes underscore a key methodological principle for large-scale MRV frameworks: remote sensing products and global databases cannot be applied as universal substitutes for all model inputs. While continuous meteorological drivers and relatively stable soil physical parameters, such as clay content, may be reliably replaced by open-access reanalysis or gridded datasets, the initial SOC baseline (SOC_0) remains a critical parameter that requires empirical ground-truthing. This is particularly important in restored or heavily disturbed systems, where historical management legacies, organic amendments, soil reconstruction practices, and local contamination-remediation actions may generate baseline SOC stocks that strongly deviate from the natural biogeochemical carrying capacity of the system. In such cases, process-based models such as RothC may reproduce the general direction of SOC change, but they cannot fully recreate SOC dynamics under all situations, especially when the initial carbon stock is far above what the soil, vegetation, and bioclimatic conditions can sustain over the long term. Therefore, accurate baseline sampling is essential not only for model initialisation, but also for interpreting whether subsequent SOC losses reflect model failure, ecosystem degradation, or a natural adjustment towards a new equilibrium state. These findings highlight the need to combine field observations, remote sensing products, and process-based simulations within a carefully validated framework, rather than treating spatial datasets as direct replacements for local soil information.

4.2. Landscape

The landscape-scale simulation provides a complementary perspective to the plot-based boundary condition analysis. However, it is important to emphasise that this approach was not based on SOC measurements. Instead, all input variables were derived from remote sensing products, climate reanalysis data, and global soil databases. In particular, the SOC values used to initialise the year 2000 baseline were obtained from SoilGrids, representing an attempt to reconstruct the spatial baseline condition of the Guadiamar Green Corridor using globally available soil information. Therefore, the landscape analysis should be interpreted as a spatially explicit modelling exercise based on open-access

datasets, rather than as a direct reconstruction of measured SOC stocks across the restoration area. Under this configuration, the model simulated an overall increase in SOC stocks between 2000 and 2024, with most of the landscape acting as a carbon sink. This result contrasts with some of the plot-scale observations, where several sampling plots showed a decline in SOC over the same period. This apparent discrepancy is mainly explained by the different nature of the baseline used in each analysis. At plot scale, the 2000 baseline reflected field-measured SOC stocks shortly after remediation, when large amounts of organic and clay-rich amendments had been applied to the most contaminated areas. These initial SOC values were therefore strongly influenced by local restoration practices and, in several plots, were considerably higher than what the soil–vegetation–climate system could sustain over the long term. By contrast, the SoilGrids-derived baseline used in the landscape simulation represents a modelled regional estimate of SOC, which is more likely to reflect broader edaphoclimatic conditions than the highly localised effects of post-spill amendment applications.

This distinction is critical for interpreting the results. The positive SOC balance obtained at landscape scale does not necessarily contradict the SOC decline observed in some field plots. Rather, it suggests that, when initial SOC stocks are defined from a global soil product and driven by remotely sensed productivity and reanalysis climate data, the Guadiamar landscape has the potential to function as a moderate carbon sink under current vegetation and climatic conditions. In other words, the landscape simulation represents the expected SOC trajectory under a harmonised, gridded baseline, whereas the sub-landscape analysis captures the legacy of site-specific remediation actions and the subsequent relaxation of artificially elevated SOC stocks towards a new equilibrium.

The use of SoilGrids as the baseline dataset also introduces an important methodological limitation. Global digital soil mapping products are designed to provide spatially continuous estimates over large areas, but they may not capture abrupt, localised or anthropogenic soil modifications, such as those associated with mining-spill remediation, topsoil removal, clay amendment application or organic amendment incorporation. This reinforces the conclusion obtained from the boundary condition analysis: global soil datasets can be useful for regional modelling where field data are unavailable, but their outputs must be interpreted cautiously in disturbed or reconstructed landscapes.

The strong relationship between simulated SOC accumulation and MODIS-derived carbon inputs further indicates that vegetation productivity was a major driver of landscape-scale SOC dynamics. MODIS GPP/NPP products are specifically designed to provide spatially continuous estimates of terrestrial vegetation productivity and are widely used for ecosystem status assessment, carbon-cycle analysis and environmental monitoring [37,46]. Areas receiving higher annual organic inputs tended to behave as carbon sinks, whereas areas with lower productivity or higher initial SOC stocks were more likely to show limited accumulation or carbon losses. This pattern should not be interpreted as direct evidence that the soils were approaching a mineral-controlled carbon saturation threshold. The study did not quantify mineral-associated organic carbon, reactive mineral surface area or carbon saturation deficit. Therefore, the negative relationship between initial SOC and subsequent simulated change is better interpreted as an initial-stock-dependent response within the RothC modelling framework. In this context, cells with higher initial SOC stocks had lower relative potential for additional simulated accumulation, whereas cells with lower initial SOC stocks showed greater simulated gains under the imposed carbon-input scenario [47,48]. Therefore, the observed relationship should be interpreted as an initial-stock-dependent response within the RothC modelling framework, rather than as direct evidence of mineral-controlled SOC saturation.

The uncertainty analysis showed that the simulated carbon sink remained relatively robust under perturbations of carbon inputs and decomposition modifiers. Nevertheless, this robustness should be understood within the assumptions of the gridded modelling framework. The relatively stable prediction interval ratio indicates internal consistency of the spatial RothC implementation, but it does not eliminate the uncertainty associated with the choice of baseline dataset. SoilGrids 2.0 provides globally consistent soil-property predictions at 250 m resolution with spatially explicit uncertainty, using machine-learning models trained on global soil observations and environmental covariates [24]. However, recent studies also highlight that global soil raster products may provide useful regional-scale information while still showing important local inaccuracies when evaluated against external soil datasets, especially in heterogeneous landscapes or areas affected by specific local processes [49]. In this sense, the largest source of uncertainty is not only the propagation of model parameters, but also the representativeness of the initial SOC map used to initialise the simulation. This limitation is particularly relevant in the Guadiamar Green Corridor, where the year 2000 baseline derived from SoilGrids represents a modelled regional approximation rather than a field-measured post-remediation SOC inventory.

Overall, the landscape analysis demonstrates the potential of combining SoilGrids, OpenLandMap, ERA5-Land and MODIS-derived productivity data to implement spatially explicit RothC simulations in areas where complete field datasets are unavailable. However, the results should be interpreted as a regional modelling scenario based on remote sensing and global baseline products, not as a direct substitute for field-based SOC monitoring. For restored and anthropogenically disturbed systems such as the Guadiamar Green Corridor, landscape-scale simulations are most valuable when used together with plot-scale observations, allowing the identification of discrepancies between modelled background SOC trajectories and local soil dynamics shaped by remediation history.

5. Conclusions

This study evaluated how alternative soil and climate datasets influence RothC simulations of long-term SOC dynamics at plot and landscape scales in the Guadiamar Green Corridor. Field observations suggested a decline in surface-layer SOC by 2024, although this result should be interpreted cautiously because the 2024 campaign focused on the 0–20 cm topsoil layer. Model performance was most consistent in riparian woodland, whereas shrubland showed greater variability. The initial SOC stock was identified as the input with the greatest influence on the simulated trajectories.

At the sub-landscape scale, model performance varied among land-cover categories and boundary-condition scenarios. Riparian woodland showed the most consistent model performance, whereas shrubland showed greater variability. The grassland results should be interpreted as site-specific because this land-cover category was represented by only one independent monitoring plot. The boundary-condition analysis showed that not all RothC input variables have the same influence on model performance. Replacing the initial SOC baseline produced the largest deterioration in model performance, whereas the alternative climate configuration used in BC6 provided the most consistent overall results. This indicates that the representativeness of the initial SOC stock is a critical requirement for RothC application in restored and anthropogenically disturbed soils.

The results therefore show that remote sensing products and global environmental datasets can support SOC modelling, but they cannot be applied as universal replacements for field data. This is especially relevant in restored or anthropogenically disturbed systems, where local management history, soil reconstruction and amendment application may generate SOC stocks that differ markedly from the values expected under natural soil, vegetation and bioclimatic conditions. Under these circumstances, process-based models may

capture broad tendencies, but they cannot be expected to fully reproduce all SOC dynamics when the baseline state is strongly influenced by remediation and amendment application.

At landscape scale, the spatial RothC implementation provided a complementary regional perspective based on gridded datasets. However, the simulated regional SOC increase contrasted with the decline observed in the field plots. This difference was mainly associated with the use of a globally modelled SOC baseline at landscape scale, which did not fully represent the legacy of soil remediation and amendment application captured by the field observations. The spatial simulation should therefore be interpreted as an open-dataset-driven modelling scenario rather than as a direct reconstruction of field-observed SOC changes across the Guadiamar Green Corridor.

The uncertainty analysis indicated that the spatial model was internally robust under perturbations of carbon inputs and decomposition modifiers. Nevertheless, the main source of uncertainty remains the representativeness of the initial SOC map used to initialise the simulations. Global soil products such as SoilGrids can therefore support regional screening in data-scarce contexts, but their outputs should be validated against field observations in areas affected by strong local disturbance or restoration interventions.

Overall, this study supports the use of RothC, remote sensing and open-access environmental datasets as complementary tools for scalable SOC monitoring. However, it also demonstrates that robust SOC modelling in restored landscapes requires a hybrid framework in which field measurements are used to constrain and validate model baselines, while remote sensing and gridded datasets provide spatial continuity and temporal consistency. In Mediterranean restoration contexts such as the Guadiamar Green Corridor, this combined approach is essential to distinguish between real ecosystem degradation, natural SOC stabilisation after remediation, and model uncertainty arising from baseline assumptions.

Author Contributions: Conceptualization, J.B.-G.; methodology, J.B.-G.; software, J.B.-G.; validation, J.B.-G., J.M.C.-N. and F.J.B.-V.; formal analysis, J.B.-G.; investigation, J.B.-G.; resources, J.B.-G., F.J.B.-V. and M.A.-R.; data curation, J.B.-G.; writing—original draft preparation, J.B.-G.; writing—review and editing, J.B.-G., J.M.C.-N., F.J.B.-V. and M.A.-R.; visualization, J.B.-G.; supervision, M.A.-R. and J.M.C.-N.; project administration, J.B.-G. and M.A.-R.; funding acquisition, M.A.-R. All authors have read and agreed to the published version of the manuscript.

Funding: This research was funded by the European Commission through the MRV4SOC project, under grant number 101112754.

Data Availability Statement: The Rstudio code used to run the model could be found here: https://zenodo.org/records/20378987 (accessed on 20 June 2026).

Acknowledgments: We thank the MRV4SOC team for their support during manuscript preparation and project development. The MRV4SOC project is supported by the European Commission's Horizon Europe Programme under Grant Agreement No. 101112754.

Conflicts of Interest: Authors Javier Bravo-García, Francisco José Blanco-Velázquez, María Anaya-Romero were employed by the company Evenor-Tech (Spain). The remaining authors declare that the research was conducted in the absence of any commercial or financial relationships that could be construed as a potential conflict of interest.

Abbreviations

The following abbreviations are used in this manuscript:

SOC	Soil organic carbon
SDGs	Sustainable Development Goals
MRV	Monitoring, reporting and verification
RothC	Rothamsted Carbon Model

BC	Boundary condition
RS	Remote sensing
GEE	Google Earth Engine
NDVI	Normalised Difference Vegetation Index
fPAR	Fraction of absorbed photosynthetically active radiation
APAR	Absorbed photosynthetically active radiation
NPP	Net primary productivity
MODIS	Moderate Resolution Imaging Spectroradiometer
MOD17A3HGF	MODIS annual gap-filled gross and net primary productivity product
ERA5	ECMWF Reanalysis v5 Land dataset
ECMWF	European Centre for Medium-Range Weather Forecasts
C3S	Copernicus Climate Change Service
BIO	Microbial biomass
HUM	Humified organic matter
DPM	Decomposable plant material
RPM	Resistant plant material
DR	DPM/RPM ratio
IOM	Inert organic matter
GPP	Gross primary productivity
ET	Evapotranspiration
ETP	Potential evapotranspiration
RMSE	Root mean square error
EF	Nash–Sutcliffe efficiency coefficient
PBIAS	Percentage bias
PIR	Prediction interval ratio
STD	Standard deviation
UTM	Universal Transverse Mercator

References

1. Koorneef, G.J.; Pulleman, M.M.; Comans, R.N.; van Rijssel, S.Q.; Barré, P.; Baudin, F.; de Goede, R.G. Assessing soil functioning: What is the added value of soil organic carbon quality measurements alongside total organic carbon content? *Soil Biol. Biochem.* **2024**, *196*, 109507. [CrossRef]
2. Bossio, D.A.; Cook-Patton, S.C.; Ellis, P.W.; Fargione, J.; Sanderman, J.; Smith, P.; Wood, S.; Zomer, R.J.; von Unger, M.; Emmer, I.M.; et al. The role of soil carbon in natural climate solutions. *Nat. Sustain.* **2020**, *3*, 391–398. [CrossRef]
3. Smith, P.; Soussana, J.-F.; Angers, D.; Schipper, L.; Chenu, C.; Rasse, D.P.; Batjes, N.H.; van Egmond, F.; McNeill, S.; Kuhnert, M.; et al. How to measure, report and verify soil carbon change to realize the potential of soil carbon sequestration for atmospheric greenhouse gas removal. *Glob. Chang. Biol.* **2020**, *26*, 219–241. [CrossRef] [PubMed]
4. Sommer, R.; Bossio, D. Dynamics and climate change mitigation potential of soil organic carbon sequestration. *J. Environ. Manag.* **2014**, *144*, 83–87. [CrossRef] [PubMed]
5. Smith, P. Do grasslands act as a perpetual sink for carbon? *Glob. Chang. Biol.* **2014**, *20*, 2708–2711. [CrossRef] [PubMed]
6. Madejón, P.; Domínguez, M.T.; Madejón, E.; Cabrera, F.; Marañón, T.; Murillo, J.M. Soil-plant relationships and contamination by trace elements: A review of twenty years of experimentation and monitoring after the Aznalcóllar (SW Spain) mine accident. *Sci. Total. Environ.* **2018**, *625*, 50–63. [CrossRef] [PubMed]
7. Baier, C.; Modersohn, A.; Jalowy, F.; Glaser, B.; Gross, A. Effects of recultivation on soil organic carbon sequestration in abandoned coal mining sites: A meta-analysis. *Sci. Rep.* **2022**, *12*, 20090. [CrossRef] [PubMed]
8. Song, W.; Li, J.; Li, X.; Xu, D.; Min, X. Effects of land reclamation on soil organic carbon and its components in reclaimed coal mining subsidence areas. *Sci. Total. Environ.* **2023**, *908*, 168523. [CrossRef] [PubMed]
9. Fowler, A.F.; Basso, B.; Millar, N.; Brinton, W.F. A simple soil mass correction for a more accurate determination of soil carbon stock changes. *Sci. Rep.* **2023**, *13*, 2242. [CrossRef] [PubMed]
10. Soria, R.; de la Rosa, J.M.; González-Pérez, J.A.; Bastida, F.; Ortega, R.; Miralles, I. Assessing organic amendments for improving SOM dynamics and microbial functioning in degraded quarry soils. *Environ. Technol. Innov.* **2025**, *39*, 104323. [CrossRef]
11. van Wesemael, B.; Chabrillat, S.; Dias, A.S.; Berger, M.; Szantoi, Z. Remote Sensing for Soil Organic Carbon Mapping and Monitoring. *Remote Sens.* **2023**, *15*, 3464. [CrossRef]

12. Sabetizadeh, M.; Zhou, Y.; Heinesch, B.; Longdoz, B.; Beauclaire, Q.; van Wesemael, B. Assessing Soil Organic Carbon Dynamics Across Croplands and Grasslands: A RothC Model Analysis with Varied Carbon Inputs. In Proceedings of the EGU General Assembly 2025, Vienna, Austria, 27 April–2 May 2025. EGU25-19111. [CrossRef]
13. European Commission. *EU Soil Strategy for 2030: Reaping the Benefits of Healthy Soils for People, Food, Nature and Climate*; COM (2021) 699 final; European Commission: Brussels, Belgium, 2021.
14. Coleman, K.; Jenkinson, D.S. RothC-26.3—A Model for the turnover of carbon in soil. In *Evaluation of Soil Organic Matter Models Using Existing Long-Term Datasets*; NATO ASI Series; Powlson, D.S., Smith, P., Smith, J.U., Eds.; Springer: Berlin/Heidelberg, Germany, 1996; Volume 38, pp. 237–246. [CrossRef]
15. Maas, E.D.; Lal, R.A. A case study of the RothC soil carbon model with potential evapotranspiration and remote sensing model inputs. *Remote Sens. Appl. Soc. Environ.* **2022**, *29*, 100876. [CrossRef]
16. Metrikaitytė Gudelė, G.; Sužiedelytė Visockienė, J. Quantifying Soil Carbon Sequestration Potential Through Carbon Farming Practices with RothC Model Adapted to Lithuania. *Land* **2025**, *14*, 1497. [CrossRef]
17. Schils, R.; Dekker, C.; Oenema, J.; Hilhorst, G.; Wagenaar, J.-P.; Verloop, K. Measuring and Modeling Soil Carbon Changes on Dutch Dairy Farms. *Land* **2025**, *14*, 874. [CrossRef]
18. Samarinas, N.; Tsakiridis, N.L.; Kalopesa, E.; Tziolas, N. An Agricultural Hybrid Carbon Model for National-Scale SOC Stock Spatial Estimation. *Environments* **2025**, *12*, 477. [CrossRef]
19. Marañón, T.; Madejón, E. El Corredor Verde del Guadiamar como estudio de caso en el proyecto europeo RECARE. *Ecosistemas* **2014**, *23*, 81–82. [CrossRef]
20. Blanco-Velázquez, F.; Muñoz-Vallés, S.; Anaya-Romero, M. Assessment of sugar beet lime measure efficiency for soil contamination in a Mediterranean Ecosystem. The case study of Guadiamar Green Corridor (SW Spain). *Catena* **2019**, *178*, 163–171. [CrossRef]
21. Grimalt, J.O.; Ferrer, M.; Macpherson, E. The mine tailing accident in Aznalcollar. *Sci. Total. Environ.* **1999**, *242*, 3–11. [CrossRef] [PubMed]
22. Radočaj, D.; Gašparović, M.; Jurišić, M. Open Remote Sensing Data in Digital Soil Organic Carbon Mapping: A Review. *Agriculture* **2024**, *14*, 1005. [CrossRef]
23. Yuzugullu, O.; Fajraoui, N.; Don, A.; Liebisch, F. Satellite-based soil organic carbon mapping on European soils using available datasets and support sampling. *Sci. Remote Sens.* **2024**, *9*, 100118. [CrossRef]
24. Poggio, L.; de Sousa, L.M.; Batjes, N.H.; Heuvelink, G.B.M.; Kempen, B.; Ribeiro, E.; Rossiter, D. SoilGrids 2.0: Producing soil information for the globe with quantified spatial uncertainty. *Soil* **2021**, *7*, 217–240. [CrossRef]
25. FAO. *Measuring and Modelling Soil Carbon Stocks and Stock Changes in Livestock Production Systems: Guidelines for Assessment*; Version 1; Food and Agriculture Organization of the United Nations: Rome, Italy, 2019.
26. Alonso, C.; Antón-Pacheco, C.; Barettino, D.; Cabrera, F.; Fernández, A.M.; Fernández, J.E.; García-Gutiérrez, M.; Giraldez, J.V.; Giron, I.F.; Lopez Pamo, E.; et al. Los suelos del Guadiamar: Estudios de caracterización y de la evolución de los suelos contaminados por el lodo. *Bol. Geol. Min.* **2001**, *112*, 163–192.
27. Madejón, P.; Marañón, T.; Murillo, J.M.; Robinson, B. White poplar (*Populus alba*) as a biomonitor of trace elements in contaminated riparian forests. *Environ. Pollut.* **2004**, *132*, 145–155. [CrossRef] [PubMed]
28. Walkley, A.; Black, I.A. An examination of the Degtjareff method for determining soil organic matter, and a proposed modification of the chromic acid titration method. *Soil Sci.* **1934**, *37*, 29–38. [CrossRef]
29. Muñoz-Rojas, M. Soil Quality Indicators in Mediterranean Environments: The Guadiamar Green Corridor Case Study. Ph.D. Thesis, University of Seville, Seville, Spain, 2010.
30. Pesce, S.; Balugani, E.; De Paz, J.M.; Marazza, D.; Visconti, F. A Modified Version of RothC to Model the Direct and Indirect Effects of Rice Straw Mulching on Soil Carbon Dynamics, Calibrated in Two Valencian Citrus Orchards. *Soil Syst.* **2024**, *8*, 12. [CrossRef]
31. Geremew, B.; Tadesse, T.; Bedadi, B.; Gollany, H.T.; Tesfaye, K.; Aschalew, A.; Tilaye, A.; Abera, W. Evaluation of RothC model for predicting soil organic carbon stock in north-west Ethiopia. *Environ. Chall.* **2024**, *15*, 100909. [CrossRef]
32. Jenkinson, D.S.; Andrew, S.P.S.; Lynch, J.M.; Goss, M.J.; Tinker, P.B. The turnover of organic carbon and nitrogen in soil. *Philos. Trans. R. Soc. B Biol. Sci.* **1990**, *329*, 361–368. [CrossRef]
33. Gottschalk, P.; Smith, J.; Wattenbach, M.; Bellarby, J.; Stehfest, E.; Arnell, N.; Osborn, T.J.; Jones, C.; Smith, P. How will organic carbon stocks in mineral soils evolve under future climate? Global projections using RothC for a range of climate change scenarios. *Biogeosciences* **2012**, *9*, 3151–3171. [CrossRef]
34. Smith, P.; Falloon, P. Modelling refractory soil organic matter. *Biol. Fertil. Soils* **2000**, *30*, 388–398. [CrossRef]
35. Six, J.; Conant, R.T.; Paul, E.A.; Paustian, K. Stabilization mechanisms of soil organic matter: Implications for C-saturation of soils. *Plant Soil* **2002**, *241*, 155–176. [CrossRef]
36. Sims, D.A.; Gamon, J.A. Relationships between leaf pigment content and spectral reflectance across a wide range of species, leaf structures and developmental stages. *Remote Sens. Environ.* **2002**, *81*, 337–354. [CrossRef]

37. Running, S.W.; Thornton, P.E.; Nemani, R.; Glassy, J.M. Global terrestrial gross and net primary productivity from the earth observing system. In *Methods in Ecosystem Science*; Sala, O.E., Jackson, R.B., Mooney, H.A., Howarth, R.W., Eds.; Springer: New York, NY, USA, 2000; pp. 44–57. [CrossRef]
38. Gilmanov, T.; Soussana, J.; Aires, L.; Allard, V.; Ammann, C.; Balzarolo, M.; Barcza, Z.; Bernhofer, C.; Campbell, C.; Cernusca, A.; et al. Partitioning European grassland net ecosystem CO_2 exchange into gross primary productivity and ecosystem respiration using light response function analysis. *Agric. Ecosyst. Environ.* **2007**, *121*, 93–120. [CrossRef]
39. Beer, C.; Reichstein, M.; Tomelleri, E.; Ciais, P.; Jung, M.; Carvalhais, N.; Rödenbeck, C.; Arain, M.A.; Baldocchi, D.; Bonan, G.B.; et al. Terrestrial gross carbon dioxide uptake: Global distribution and covariation with climate. *Science* **2010**, *329*, 834–838. [CrossRef] [PubMed]
40. He, N.; Wen, D.; Zhu, J.; Tang, X.; Xu, L.; Zhang, L.; Hu, H.; Huang, M.; Yu, G. Vegetation carbon sequestration in Chinese forests from 2010 to 2050. *Glob. Chang. Biol.* **2016**, *23*, 1575–1584. [CrossRef] [PubMed]
41. FAO. *Carbon Sequestration in Dryland Soils*; World Soil Resources Reports No. 102; Food and Agriculture Organization of the United Nations: Rome, Italy, 2004.
42. Muñoz-Sabater, J. ERA5-Land Monthly Averaged Data from 1981 to Present. Copernicus Climate Change Service Climate Data Store. 2019. Available online: https://doi.org/10.24381/cds.68d2bb30 (accessed on 24 May 2026). [CrossRef]
43. De Frenne, P.; Zellweger, F.; Rodríguez-Sánchez, F.; Scheffers, B.R.; Hylander, K.; Luoto, M.; Vellend, M.; Verheyen, K.; Lenoir, J. Global buffering of temperatures under forest canopies. *Nat. Ecol. Evol.* **2019**, *3*, 744–749. [CrossRef] [PubMed]
44. Lenk, A.; Richter, R.; Kretz, L.; Wirth, C. Effects of canopy gaps on microclimate, soil biological activity and their relationship in a European mixed floodplain forest. *Sci. Total. Environ.* **2024**, *941*, 173572. [CrossRef] [PubMed]
45. Domínguez, M.T.; Marañón, T.; Murillo, J.M.; Schulin, R.; Robinson, B.H. Trace element accumulation in woody plants of the Guadiamar Valley, SW Spain: A large-scale phytomanagement case study. *Environ. Pollut.* **2008**, *152*, 50–59. [CrossRef] [PubMed]
46. Zhao, M.; Heinsch, F.A.; Nemani, R.R.; Running, S.W. Improvements of the MODIS terrestrial gross and net primary production global data set. *Remote Sens. Environ.* **2005**, *95*, 164–176. [CrossRef]
47. Georgiou, K.; Angers, D.; Champiny, R.E.; Cotrufo, M.F.; Craig, M.E.; Doetterl, S.; Grandy, A.S.; Lavallee, J.M.; Lin, Y.; Lugato, E.; et al. Soil Carbon Saturation: What Do We Really Know? *Glob. Chang. Biol.* **2025**, *31*, e70197. [CrossRef] [PubMed]
48. Breure, T.S.; De Rosa, D.; Panagos, P.; Cotrufo, M.F.; Jones, A.; Lugato, E. Revisiting the soil carbon saturation concept to inform a risk index in European agricultural soils. *Nat. Commun.* **2025**, *16*, 2538. [CrossRef] [PubMed]
49. Flynn, T.; Kostecki, R.; Rebi, A.; Raza, T. Accessing global soil raster images and equal-area splines to estimate soil organic carbon stocks on the regional scale. *Pedosphere* **2024**, *35*, 834–845. [CrossRef]

Disclaimer/Publisher's Note: The statements, opinions and data contained in all publications are solely those of the individual author(s) and contributor(s) and not of MDPI and/or the editor(s). MDPI and/or the editor(s) disclaim responsibility for any injury to people or property resulting from any ideas, methods, instructions or products referred to in the content.